Characteristics of two distinct high-light acclimated algal communities during advanced stages of sea ice melt

ARTICLE *in* POLAR BIOLOGY · DECEMBER 2011

Impact Factor: 1.59 · DOI: 10.1007/s00300-011-0998-x

Polar Biol (2011) 34:1869–1886
DOI 10.1007/s00300-011-0998-x

ORIGINAL PAPER

Characteristics of two distinct high-light acclimated algal communities during advanced stages of sea ice melt

C. J. Mundy · Michel Gosselin · Jens K. Ehn · Claude Belzile · Michel Poulin · Eva Alou · Suzanne Roy · Haakon Hop · Sylvie Lessard · Tim N. Papakyriakou · David G. Barber · Jeremy Stewart

Received: 24 September 2010 / Revised: 15 March 2011 / Accepted: 17 March 2011 / Published online: 20 April 2011

Abstract Biological characteristics of ice-associated algal communities were studied in Darnley Bay (western Canadian Arctic) during a 2-week period in July 2008 when the landfast ice cover had reached an advanced stage of melt. We found two distinct and separate algal communities: (1) an interior ice community confined to brine channel networks beneath white ice covers; and (2) an ice melt water community in the brackish waters of both surface melt ponds and the layer immediately below the ice cover. Both communities reached maximum chlorophyll *a* concentrations of about 2.5 mg m^{-3}, but with diatoms dominating the interior ice while flagellates dominated the melt water community. The microflora of each community was diverse, containing both unique and shared algal species, the latter suggesting an initial seeding of the ice melt water by the bottom ice community. Absorption characteristics of the algae indicated the presence of mycosporine-like amino acids (MAAs) and carotenoid pigments as a photoprotective strategy against being confined to high-light near-surface layers. Although likely not contributing substantially to total annual primary production, these ice-associated communities may play an important ecological role in the Arctic marine ecosystem, supplying an accessible and stable food source to higher trophic levels during the period of ice melt.

Keywords Sea ice · Melt pond · Ice algae · Photoprotection · Algal absorption · Mycosporine-like amino acid

This article belongs to the special issue "Circumpolar Flaw Lead Study (CFL)", coordinated by J. Deming and L. Fortier.

C. J. Mundy (✉) · M. Gosselin · C. Belzile · E. Alou · S. Roy · S. Lessard
Institut des sciences de la mer (ISMER), Université du Québec à Rimouski, 310 Allée des Ursulines, Rimouski, QC G5L 3A1, Canada
e-mail: Christopher-john.mundy@uqar.qc.ca

J. K. Ehn
Marine Physical Laboratory, Scripps Institution of Oceanography, University of California at San Diego, La Jolla, CA 92093-0238, USA

M. Poulin
Research Division, Canadian Museum of Nature, PO Box 3443, Station D, Ottawa, ON K1P 6P4, Canada

H. Hop
Fram Centre, Norwegian Polar Institute, 9296 Tromsø, Norway

T. N. Papakyriakou · D. G. Barber
Centre for Earth Observation Science, University of Manitoba, Winnipeg, MB R3T 2N2, Canada

J. Stewart
Fisheries and Oceans Canada, Freshwater Institute, Winnipeg, MB R3T 2N6, Canada

Introduction

Sea ice imposes a unique level of complexity to the Arctic marine ecosystem. In particular, numerous types of algal communities can be found within different habitats associated with the sea ice environment. In winter and spring, the bulk of ice algal biomass is located within the bottom few centimeters of the ice (Smith et al. 1990) and consists predominately of a pennate diatom assemblage (von Quillfeldt 2000; Różańska et al. 2009). Other ice communities mostly develop as the ice melts in late spring and summer. Horner et al. (1992) defined four communities based on their vertical location within the ice, which included surface, interior, bottom (interstitial), and sub-ice. A fifth community referred

to as an under-ice melt pond community was described by Gradinger (1996).

During summer, sea ice in the Arctic undergoes a rapid transformation with enhanced melt rates leading to the formation of surface melt ponds and accumulation of low-salinity melt water immediately below the ice cover (Eicken et al. 2002). Sub-ice communities have been documented under Arctic pack ice and typically form mucilaginous masses or strands dominated by diatoms (Syvertsen 1991; Melnikov et al. 2002). Communities inhabiting the ice melt water, including surface and under-ice melt ponds, as well as within interior ice, have been characterized by chlorophyte and, or chrysophyte (Bursa 1963; Melnikov et al. 2002; Gradinger et al. 2005), as well as prasinophyte (Gradinger 1996) dominance. Furthermore, a so-called halocline algal community can grow along the ice melt seawater-stratified boundary layer located at ca. 2-m water depth (Apollonio 1985).

In contrast, diatom dominance in some interior ice communities has been observed (Buck et al. 1998; Gradinger 1999). Although rare for the Arctic, Buck et al. (1998) reported an infiltration community, associated with nutrient rich waters from the underlying water column. This seawater source was in stark contrast to the low-salinity conditions associated with ice melt water (Gradinger et al. 2005).

Early summer is also a time of peak solar insolation. Disappearance of the snow cover and development of melt ponds greatly increase the amount of light transmitted through the sea ice (Perovich 2005). Surface stratification enables the ice-associated communities to stay within the upper meters of the water column in a 24-h high-light environment. The surface melt pond community in particular is subject to very high light levels, compounded by reflection from the ice surface.

Very little is known about photoacclimative responses of ice melt water-associated communities to protect against potentially harmful radiation levels. Active photoprotective strategies of marine microbes to protect against harmful radiation levels include the production of screening and quenching compounds (Kirk 1994; Roy 2000). Indeed, production of photoprotective carotenoids by Arctic bottom ice algae in response to increasing light levels in late spring has been observed (Kashino et al. 1998; Kudoh et al. 2003; Leu et al. 2010). Furthermore, mycosporine-like amino acids (MAAs), important ultraviolet radiation (UVR) screening compounds, have been noted to occur in relatively high quantities within interior ice communities of the Baltic Sea (Uusikivi et al. 2010).

Until now, the algal communities developing in the different habitats during the melt season (i.e., surface melt ponds, ice interior, sub-ice, under-ice melt ponds, and under-ice halocline) have never been studied simultaneously within landfast first-year sea ice. Here, we accomplish this task on samples from advanced stages of melting ice over an 11-day period from June 8 to 18, 2008. We describe the communities and their habitats and provide evidence that in the system we observed, the ice melt water habitats (i.e., surface melt ponds, under-ice melt pond, and halocline communities) may not be distinct from each other. Furthermore, we discuss some of the photoprotective strategies employed by these communities inferred from particulate absorption measurements.

Materials and methods

Study site

All data were collected from landfast first-year sea ice in Darnley Bay, a coastal Arctic bay along the southern shore of Amundsen Gulf onboard the CCGS *Amundsen* between June 8 and 18, 2008 (69°49.5′ N, 123°38.0′ W; Mundy et al. 2009); the site was relocated on June 18 by 1.2 km southwest (69°48.9′ N, 123°39.0′ W) due to a receding ice edge during the study. Physical progression of the sea ice melt and its effect on spectral transmittance of photosynthetically active radiation (PAR) during our study have been described by Ehn et al. (in press). Throughout the study, the sea ice was covered by melt ponds separated by white ice mounds (defined as the drained, highly reflective, melting ice surface surrounding melt ponds).

Sample collection

Samples were collected from distinct locations, as depicted schematically on a north (0 m) to south (24 m) ice-thickness transect measured on June 13 (Ehn et al. in press; Fig. 1). While on site, multiple ice cores were collected for

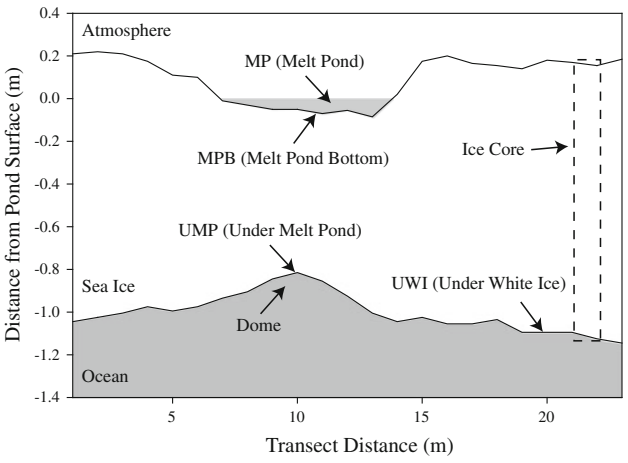

Fig. 1 A diagrammatic representation of the sampling scheme overlain on a north (0 m) to south (24 m) ice-thickness transect measured on June 13 as presented by Ehn et al. (in press)

physical and biological measurements on a white ice mound on June 9, 12, and 18. Ice cores were extracted from white ice using a 9-cm ice corer (Mark II Coring System, Kovacs Enterprises), then sectioned and transferred into isothermal containers as quickly as possible to minimize brine drainage of the samples. However, we note that some drainage may have occurred, which would affect salinity and some biological measurements. Melt water samples were collected on June 8, 11, and 18 with a modified 3.5-L Trident® suction (slurp) gun from surface melt ponds (MP) and from the melt pond bottom (MPB). In addition, melt water was collected under the ice with the aid of SCUBA divers along the sub-ice surface under melt ponds (UMP) and under white ice (UWI) and within the under-ice dome that is created below a melt pond (dome) (Fig. 1). MP and dome samples were collected by suspending the slurp gun nozzle approximately 5 cm from the ice surface and bottom, respectively, whereas the MPB, UMP, and UWI were collected by dragging the slurp gun nozzle flat along the ice surface and bottom while collecting the sample in the gun with its piston before closing with a stopper. All samples were stored in isothermal containers, protected from sunlight and brought back to the ship for processing.

Environmental measurements

Downwelling incident ultraviolet-A (UVA, 315–400 nm) and ultraviolet-B (UVB, 280–315 nm) radiation (UVR = UVA + UVB; UVS-AB-T, Kipp & Zonen), and PAR (400–700 nm; PARLite, Kipp & Zonen) were monitored on a tower at the bow of the ship prior to and during the study period. During the study, the ship moved between the adjacent bays, Darnley Bay and Franklin Bay. Due to the relatively small distance covered by the ship during the study (ca. 50 km between sites), we assumed the incident radiation was representative for the study.

A conductivity probe (Cond 330i, WTW) was used to determine salinity of melt water samples. Ice core bulk salinity and temperature measurements have been presented by Ehn et al. (in press). Equations reviewed by Petrich and Eicken (2010) were used to calculate brine salinity and volume from these measurements. Brine salinity and volume were then interpolated to the resolution used in the biological ice samples.

Silicic acid, phosphate, and nitrite + nitrate were determined on the ship with a Bran-Luebbe III nutrient autoanalyzer (adapted from Grasshoff et al. 1999) for bottom ice samples and all melt water samples. A simple linear correction for the effect of varying salinity was made for silicic acid and phosphate concentrations, as recommended by Grasshoff et al. (1999). Prior to nutrient analysis, samples were filtered through pre-combusted Whatman GF/F filters. For sea ice nutrient analysis, a separate ice core was extracted and the bottom 0–3 and 3–10-cm sections were collected and melted slowly in the dark in sterile bags (Nasco Whirl–pak®) over a 24-h period.

Algal community analysis

Additional ice cores were collected for biological analyses. A single ice core was cut into sections starting from the bottom 0–3, 3–10, 10–20 cm and then 20-cm sections until the surface section of the ice core that was <20 cm and variable in size. Four to six additional bottom ice (0–3 and 3–10 cm) core sections were pooled with the original bottom sections to provide enough material for different studies using the same samples. All ice core samples collected for particulate measurements were diluted at ca. 3:1 with 0.2-μm-filtered seawater to minimize osmotic shock of the microbial community while melting (Garrison and Buck 1986).

Subsamples were taken from ice and ice melt water samples for the determination of chlorophyll (Chl) *a* concentration via fluorometry and of cell abundance of pico- (<2 μm) and nano-sized (2–20 μm) photosynthetic cells, as well as heterotrophic bacteria via flow cytometry. Duplicate subsamples (i.e., pseudo-replicates) were filtered onto Whatman GF/F filters for determination of Chl *a* concentration. The filters were placed in 90% acetone over 24 h at 5°C in the dark for pigment extraction (Parsons et al. 1984). Fluorescence of the extracted pigments was measured before and after acidification with 5% HCl using a 10-AU Turner Designs fluorometer. Chl *a* concentrations were then calculated using the equation described by Holm-Hansen et al. (1965). Four flow cytometry 5-mL subsamples were taken from each sample, screened through a 40-μm nylon cell strainer, fixed with 25% glutaraldehyde Grade I (0.1% final concentration; Sigma) in the dark at 4°C during 30 min, and then immediately frozen in liquid nitrogen (Marie et al. 2005). After at least 24 h in liquid nitrogen, subsamples were then stored at −80°C until analysis back in the Rimouski laboratory using an Epics Altra flow cytometer (Beckman Coulter). Duplicate subsamples were counted for pico- and nano-photosynthetic cells and for heterotrophic bacteria following methods described by Tremblay et al. (2009) and Belzile et al. (2008), respectively. Cells with orange fluorescence of phycoerythrin were considered as pico- and nanocyanobacteria while cells possessing only red fluorescence of chlorophyll were classified as pico- and nanoalgae. Although cryptophytes also possess phycoerythrin, their abundance as determined by microscopy never exceeded 16 cells mL^{-1} ("Appendix"). The operationally defined nanocyanobacteria were probably represented by colonies of small cells since no filamentous forms and no

cyanobacteria larger than 2 μm were observed using light microscopy. All ice core Chl *a* concentrations and cell counts were corrected for the addition of 0.2-μm-filtered seawater.

Five selected subsamples for cell identification and enumeration were preserved with acidic Lugol's solution (Parsons et al. 1984) and stored in the dark at 4°C until analysis. Cells ≥2 μm were identified to the lowest possible taxonomic rank using inverted microscopy according to Lund et al. (1958). At least 400 cells were enumerated over a minimum of three transects (Lund et al. 1958) in each 10-mL settling chamber. The limit of detection was 4 cells mL^{-1} for sea ice samples and 1 cell mL^{-1} for dome samples. The abundance of each taxon was computed according to the equation described by Horner (2002). The main references used for cell identification were Poulin and Cardinal (1982), Medlin and Hasle (1990), Poulin (1990, 1991), Tomas (1997), Bérard-Therriault et al. (1999), von Quillfeldt (2001), and Throndsen et al. (2007).

Spectral absorption measurements

Spectral absorption coefficients were measured on selected subsamples from the ice melt water on June 8 and 18 and sea ice on June 9 and 18. Coefficients of absorption for total (a_p) algal (a_ϕ) and depigmented particulates (a_d) were determined on subsamples filtered onto Whatman GF/F filters, frozen in liquid nitrogen, and then stored at −80°C until analysis. Optical density (dimensionless) of particles concentrated on the filters was measured before (OD_{fp}) and after methanol extraction (OD_{fd}) over the spectral range of 300–800 nm, according to the method described by Bricaud and Stramski (1990), using a Perkin-Elmer Lambda 12 UV–Vis spectrophotometer equipped with a 50-mm integrating sphere (Labsphere RSA-PE-20). The following equations were used to calculate the spectral absorption coefficients:

$$a_{p,d}(\lambda) = \frac{2.303 A_f}{\beta \gamma V_f}\{[OD_{fp,fd}(\lambda) - OD_f(\lambda)] - OD_{fp,fd}(800)\}, \quad (1)$$

$$a_\phi(\lambda) = a_p(\lambda) - a_d(\lambda), \quad (2)$$

where A_f is the clearance area of the filter (m^2); V_f is the volume of subsample filtered (m^3); OD_f is the optical density of a saturated blank filter; $OD_{fp,fd}$ (800) is the optical density at 800 nm used as a correction factor where pigment absorption was assumed to be zero; γ is a dilution/expansion factor used to correct for both the addition of filtered seawater (measured) and ice expansion (assumed to be 1.1) (dimensionless); and β is the filter pathlength amplification factor calculated using the relationship described by Cleveland and Weidemann (1993) (dimensionless). Absorption coefficients were further converted to Chl *a*-specific coefficients (a_p^* and a_ϕ^*) by dividing by fluorometrically determined Chl *a* concentrations.

Results

Environment

Weather during the study period was dominated by a persistent high-pressure system centered over the Amundsen Gulf. As a result, just prior to and during the study, downwelling radiation was relatively stable and high, with the exception of some cloud cover on June 13–14 that caused a decrease in PAR and UVR (Fig. 2). Daily averaged PAR, UVA, and UVB ranged between 440–740 μmol m^{-2} s^{-1}, 3.8–5.7 W m^{-2}, and 0.23–0.37 W m^{-2}, respectively, throughout the study.

Sea ice brine salinity and volume profiles were relatively stable throughout the study period (Fig. 3a, b, respectively). Brine salinities averaged 17 ± 8 and were up to 28.7 within the interior ice. Brine volumes showed maxima in the upper interior ice layers and toward the bottom ice, averaging 14 ± 4%. In contrast, ice melt water salinities were highly variable (Fig. 4). Surface melt pond salinities ranged from 0 (MP) and 0.3 (MPB) on June 8 to 5.1 on June 18. Sub-ice melt water salinities were higher than at the surface. Salinities tended to increase from the UMP and dome samples to the UWI samples (Fig. 4). Figure 5 shows a salinity profile through a 5-cm hole in a nearby melt pond

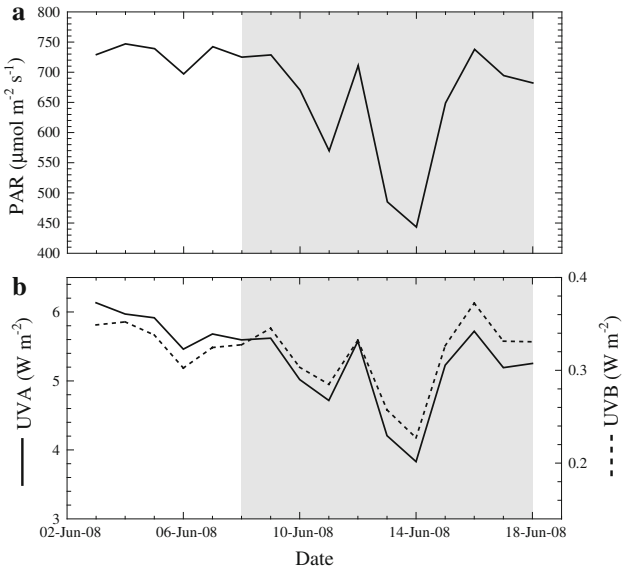

Fig. 2 Time series of daily averaged incident photosynthetically active radiation (PAR; 400–700 nm) (**a**) and UVA (315–400 nm) and UVB (280–315 nm) radiation (**b**) monitored in the southern Amundsen Gulf onboard the CCGS *Amundsen*. *Gray shading* highlights the study period, June 8–18, 2008

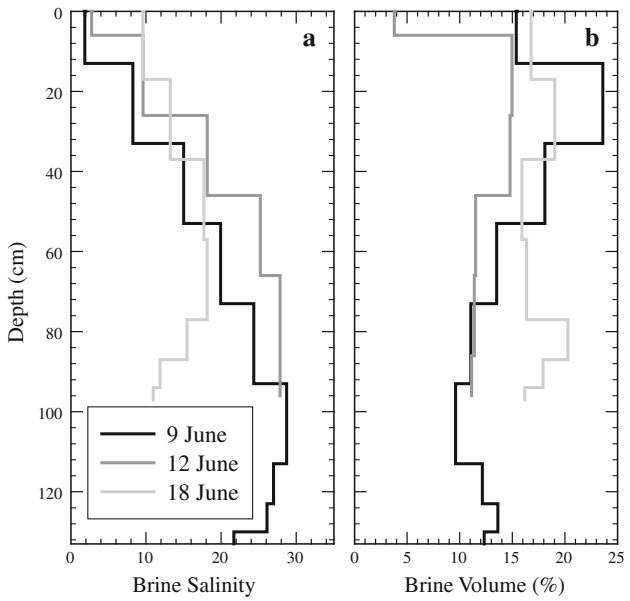

Fig. 3 Sea ice profiles of brine salinity (**a**) and volume (**b**) calculated from salinity and temperature measurements made during the study period. Note that salinity data over the bottom 10 cm on June 12 were not collected

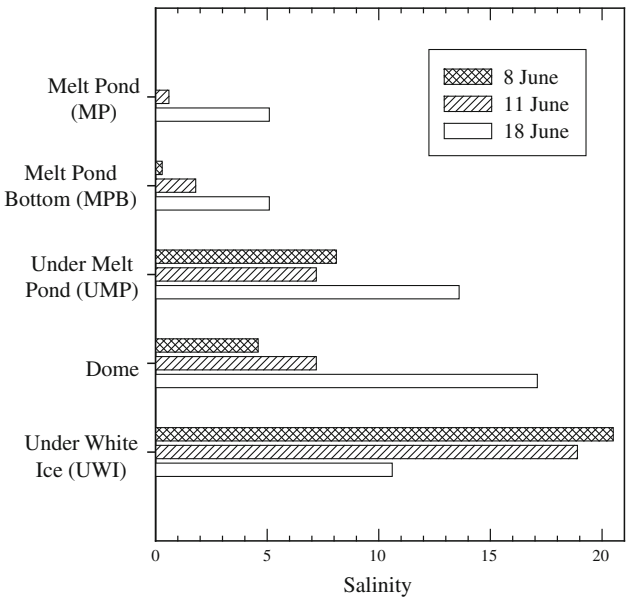

Fig. 4 Ice melt water salinities measured during the three sampling dates

over the upper 10 m of the water column collected on June 8 using a portable conductivity, temperature, and depth probe (Ocean Seven 305 CTD, Idronaut). The profile shows a distinct halocline between 1.5 and 2 m depth. Due to ice topography, the UWI samples were taken deeper into the sub-ice melt water layer (i.e., into the halocline) than the UMP and dome samples (Fig. 1). However, on June 18,

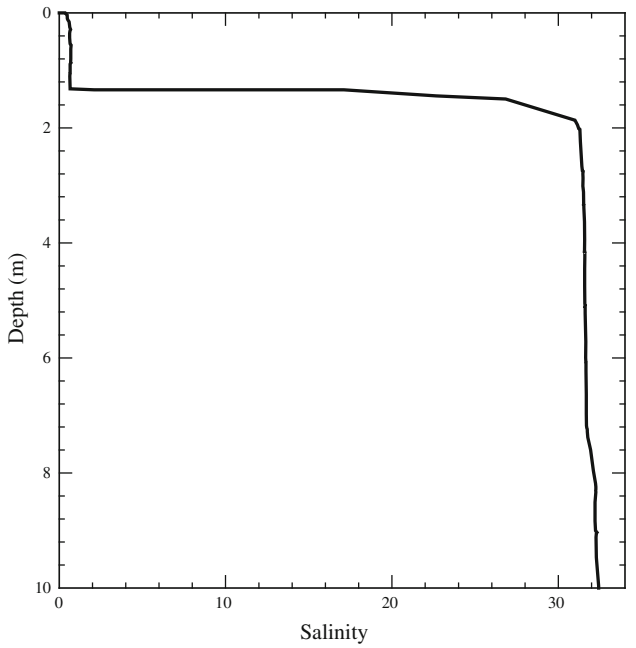

Fig. 5 Surface water column salinity profile obtained on June 8 through a 5-cm hole in the middle of a melt pond. Depth was relative to the water level in the hole

similar salinities between sub-ice samples depicted a more homogeneous sub-ice melt water layer.

Nutrient concentrations within the bottom ice and within the melt water samples were low throughout the study (Fig. 6). Corrected to brine concentrations following Manes and Gradinger (2009), silicic acid concentrations within the bottom 10 cm of the sea ice were all below detection limit (BDL). Brine phosphate concentrations ranged from BDL to 0.49 μmol L^{-1}, whereas brine concentrations of nitrite + nitrate were variable, averaging 1.69 ± 2.14 μmol L^{-1}. In the melt water samples, silicic acid and phosphate were significantly related to salinity (Fig. 6a, b, respectively). Both relationships had *y*-axis intercepts of ca. 0 μmol L^{-1} and fit close to the dilution line from observations at a 5-m water depth where salinity and silicic acid, phosphate and nitrite + nitrate concentrations averaged 31.6 ± 0.14 μmol L^{-1}, 7.58 ± 4.91 μmol L^{-1}, 0.69 ± 0.07 μmol L^{-1}, and 0.97 ± 0.67 μmol L^{-1}, respectively (data not shown). Similar to the bottom ice, nitrite + nitrate concentrations were highly variable in the melt water samples and did not correlate with salinity (Fig. 6c). On June 11, nitrite + nitrate concentrations all fell above the nitrite + nitrate dilution line for the 5-m water depth, whereas on June 8 and 18, nitrate + nitrite concentrations were much less than the dilution line. Excluding BDL measurements and those made on June 11, mean ice melt water molar ratios of 0.08 for N:Si and 0.75 for N:P were much less than observed at the 5-m water depth.

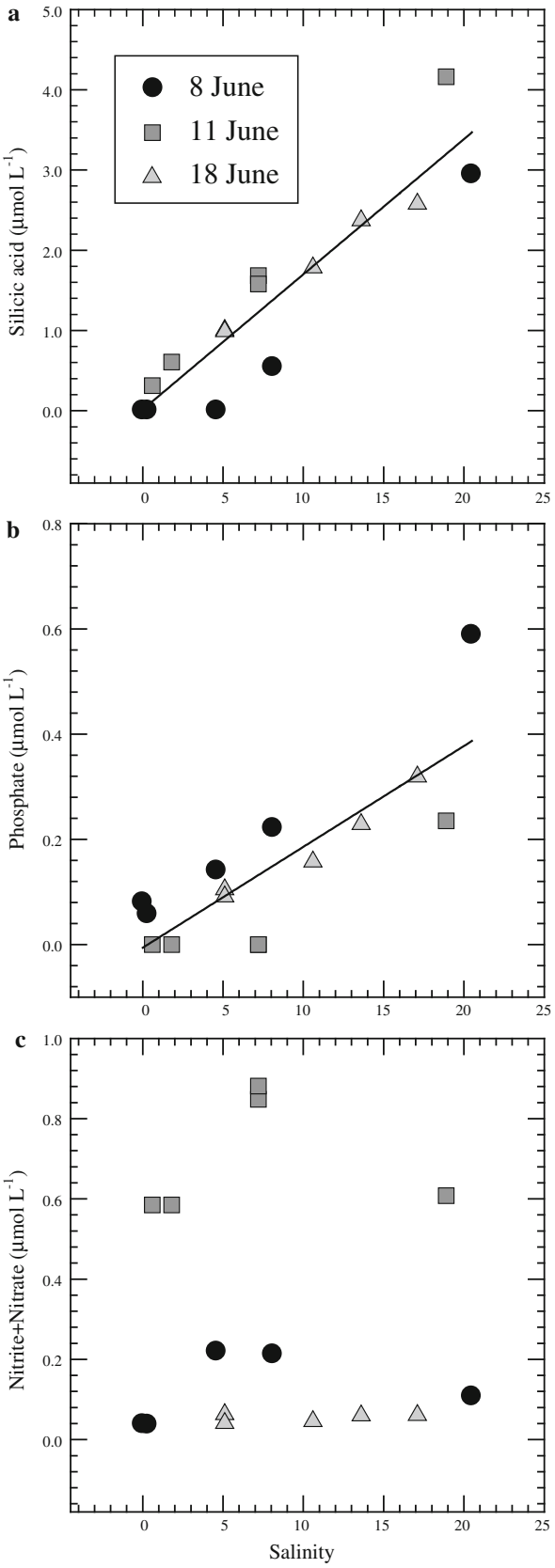

Fig. 6 Silicic acid (**a**), phosphate (**b**), and nitrite + nitrate (**c**) as a function of salinity in ice melt water during the three sampling dates

Algal community

Chl *a* concentration in sea ice varied between 0.65 and 2.6 mg m^{-3} (Fig. 7a), with integrated concentrations (1.2–1.7 mg m^{-2}) remaining fairly constant throughout the study. The vertical core sections revealed highest Chl *a* concentrations within the upper 50 cm of the ice cover associated with the brine salinity gradient and peak in brine volume (Fig. 3). Furthermore, concentrations tended to increase at the bottom of ice cores. The same vertical distribution was observed in the abundance of photosynthetic cells <20 µm (i.e., cyanobacteria and algae smaller than 20 µm; Fig. 7b). Interestingly, peaks in heterotrophic bacterial abundance occurred in the surface ice and at ca. 80 cm depth into the ice where algal biomass was minimal (Fig. 7c).

After the removal of an outlier (surface ice sample on June 12), significant positive correlations were observed between brine volume with total photosynthetic cells <20 µm ($r = 0.67$, $P < 0.001$, $n = 21$). Positive correlations of brine volume against nanoalgae ($r = 0.60$, $P < 0.01$, $n = 21$) and against Chl *a* concentration, picocyanobacteria, and nanocyanobacteria abundances were also observed; however, *P* values were only <0.05 for the latter three correlations. No correlations were observed between brine volume with picoalgae or with heterotrophic bacteria.

Nanoalgae were the dominant size group of photosynthetic cells <20 µm in the sea ice (Fig. 8). Percent contribution of picoalgae to the total abundance of photosynthetic cells <20 µm remained relatively low (<20%) within the interior ice, but increased toward the bottom ice (Fig. 8). In contrast, the percent contribution of picocyanobacteria increased substantially within the interior sea ice layers over time.

Within the ice melt water, Chl *a* concentrations ranged from 0.1 to 2.4 mg m^{-3} (Fig. 9a). Percent contribution of picoalgae to photosynthetic cells <20 µm averaged 78% in sub-ice melt water samples during the study, but ranged from 12 to 32% in surface melt ponds. In contrast to the interior ice samples, contribution of cyanobacteria was negligible in the ice melt water (<2%; data not presented). Significant linear relationships between salinity with picoalgae ($r^2 = 0.88$, $P < 0.0001$, $n = 15$) and heterotrophic bacteria ($r^2 = 0.92$, $P < 0.0001$, $n = 15$) cell abundance revealed stable and conservative mixing of these cells as the ice melt layer mixed (Fig. 9b, d). Chl *a* concentration and nanoalgae abundance were not significantly related to salinity; however, they significantly correlated with each other ($r = 0.95$, $P < 0.0001$, $n = 15$).

Taxonomic composition

Major unicellular eukaryote groups observed in the interior ice (17–37-cm section from the ice surface collected on

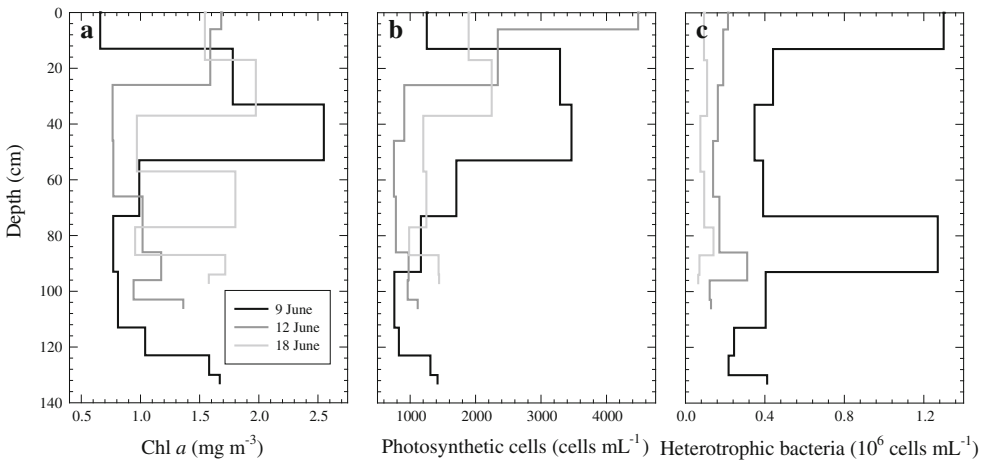

Fig. 7 Sea ice profiles of chlorophyll *a* (Chl *a*) concentration (**a**), abundance of photosynthetic cells <20 μm in diameter (**b**), and heterotrophic bacteria cell abundance (**c**) observed during the three sampling dates

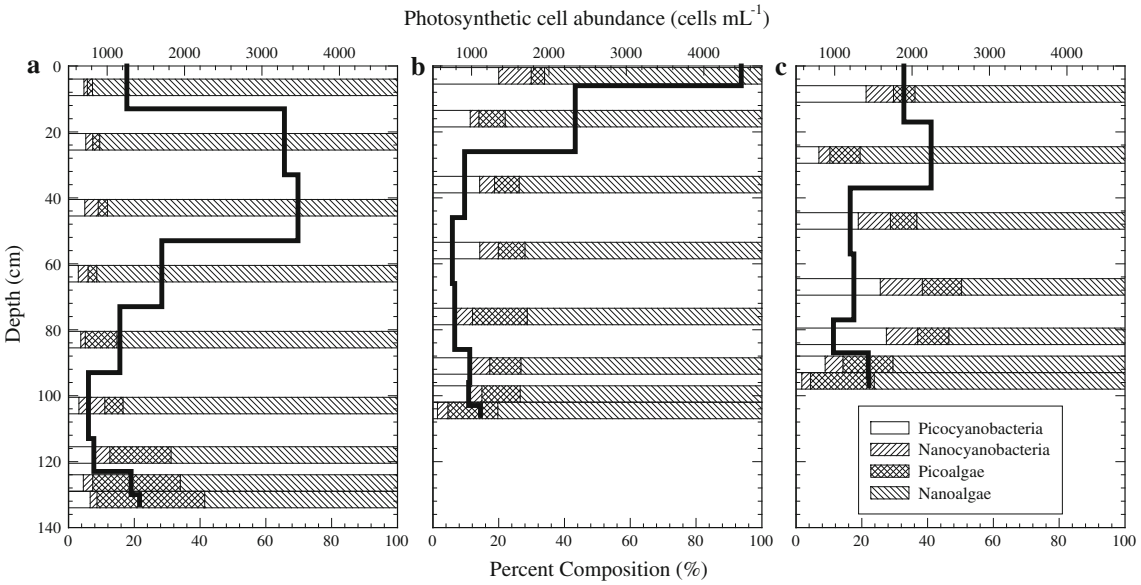

Fig. 8 Sea ice profiles of the percent composition of photosynthetic cells <20 μm in diameter (*bar plots*) observed on June 9 (**a**), 12 (**b**), and 18 (**c**), 2008. The abundance of photosynthetic cells <20 μm in diameter from Fig. 7b is included for reference (*bold lines*)

June 18), bottom ice (bottommost 3 cm collected on June 9 and 18), and dome samples (collected on June 8 and 18) are presented in Fig. 10 (refer to "Appendix" for a detailed taxonomic list). Due to the observed conservative mixing of nutrients and flow cytometry data in the ice melt water samples as well as correlations between Chl *a* and nanoalgae, dome samples were assumed to be representative of the ice melt water algal community taxonomic composition. Diatoms were the dominant group in the interior ice, accounting for 87% of the total unicellular eukaryotes. In contrast, flagellates were numerically dominant in the dome samples, ranging between 63 and 93% of total unicellular eukaryotes. Within bottom ice, flagellates were also the dominant group, ranging from 52 to 66%. It is noteworthy that the distribution of major eukaryote taxa was very similar between bottom ice and dome samples at the beginning of the study. In all samples, dinoflagellates represented a negligible fraction of the total eukaryotes (<3%).

In sea ice, pennate diatoms represented the dominant diatom group (Fig. 10). The solitary pennate diatom *Cylindrotheca closterium* and a few unidentified centric diatom species of the genus *Chaetoceros* were ubiquitous in all samples. Species unique to the sea ice included nearly all *Nitzschia* spp. and *Navicula* spp., whereas *Fragilariopsis oceanica* was unique to the dome sample. We note that *F. oceanica* accounted for 22% of the total diatom abundance of a sample taken from 34 m depth in the water column on June 18 (S. Lessard, unpubl. data).

Although unidentified flagellates accounted for 57–81% of the total flagellates enumerated, some trends were

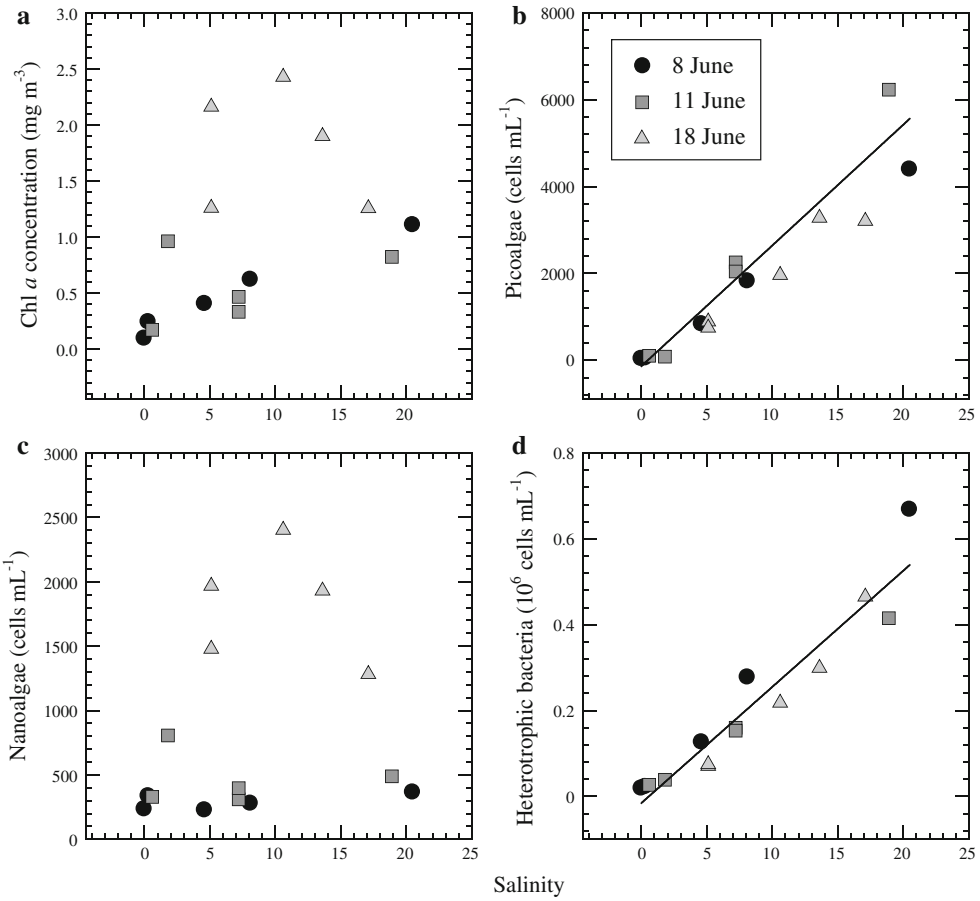

Fig. 9 Chlorophyll *a* (Chl *a*) concentration (**a**) and picoalgae (**b**), nanoalgae (**c**) and heterotrophic bacteria (**d**) abundance as a function of salinity in the ice melt water observed over the study period. *Lines* represent significant linear relationships discussed in the text

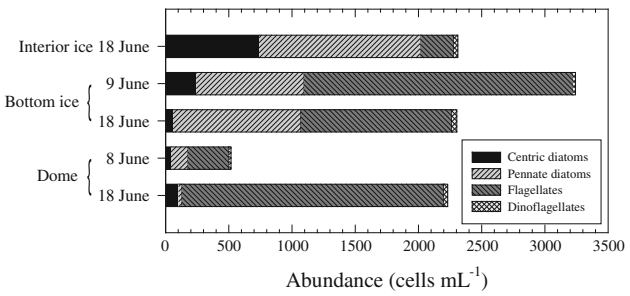

Fig. 10 Composition and abundance of major taxonomic groups of eukaryotic cells ≥2 μm in diameter (counted using inverted microscopy) in the interior ice (17–37-cm section from the ice surface collected on June 18), bottom ice (bottommost 3 cm collected on June 9 and 18) and dome samples (collected on June 8 and 18)

observed in the identified flagellates. Prasinophytes, chrysophytes, and prymnesiophytes represented >80% of all identified photosynthetic flagellate classes in both the sea ice and the dome samples, and they were evenly distributed within the interior sea ice. However, on June 18, the prymnesiophytes had decreased in both the bottom ice and the dome sample, while both the prasinophytes and the chrysophytes increased in abundance, resulting in a change of the dominant photosynthetic flagellate classes. Notably, *Pyramimonas* spp. accounted for nearly all observed prasinophytes, and *Dinobryon* spp. represented the majority of chrysophytes.

Spectral absorption

Averaged a_p^* and a_ϕ^* spectra are shown for interior ice (surface to 10 cm from the ice bottom), bottom ice (bottommost 10-cm sections), and ice melt water samples (Fig. 11). The most significant differences between the spectra were the magnitude and wavelength of absorption peaks in the UVR range. The lowest UV peaks in a_ϕ^* were observed in the interior ice and were largely limited to wavelengths between 320 and 334 nm resulting in a broad peak centered at 327 nm in the averaged spectra. Some interior ice samples did display a small bump near 360 nm, which was visible in the averaged spectra. In the melt water, UV peaks in a_ϕ^* were very high and corresponded specifically to 334 and 360 nm and were much greater in magnitude than observed in the interior ice spectra. The bottom ice absorption spectra fell in between those of the interior ice and ice melt water. Furthermore, a minor absorption peak at 310 nm was observed in a few sea ice and melt water samples. In the melt water samples, peaks

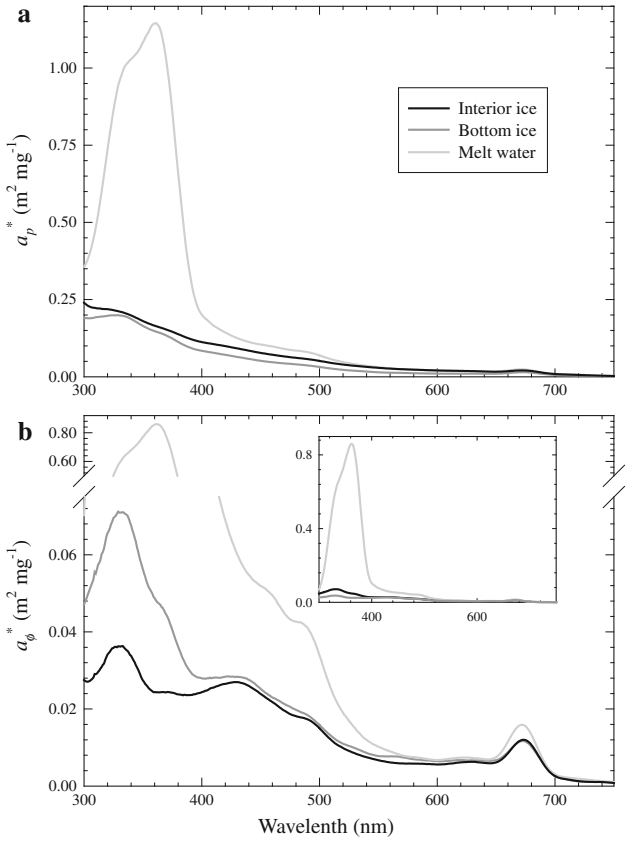

Fig. 11 Total particulate (a_p^*; **a**) and algal (a_ϕ^*; **b**) chlorophyll *a*-specific absorption spectra averaged over the study period for interior ice (surface to 10 cm from the ice bottom), bottom ice (bottommost 10 cm of the sea ice), and ice melt water samples

in a_ϕ^* at 334 and 360 nm increased between June 8 to 18 from 0.23 and 0.26–1.03 and 1.46 m^2 mg^{-1}, respectively. Furthermore, the ratio of $a_\phi(360)$:$a_\phi(334)$ increased significantly from 1.11 to 1.43 ($P < 0.0001$, $n = 10$).

In the PAR range, all spectra showed a strong absorbance shoulder centered at 490 nm (Fig. 11b), which matches peak absorption of many carotenoid pigments (Bricaud et al. 2004). Reverse phase high-performance liquid chromatography (HPLC) revealed a high contribution of photoprotective pigments within the bottom 3-cm sea ice layer (E. Alou, unpubl. data). The absorption ratio of $a_\phi(443)$:$a_\phi(490)$ has been previously used with success as an index for the contribution of photoprotective carotenoids to total absorption (Stuart et al. 2000). In our dataset, this ratio was affected by absorption tails associated with the high UV absorption peaks. We note that the absorption spectra clearly showed an inflection at 480 nm toward the 490-nm-centered shoulder (Fig. 11). Most photoprotective pigments have a spectral absorption peak at 490 nm and a trough at 480 nm (Bricaud et al. 2004). Furthermore, Johnsen et al. (1994) has shown that low-light acclimated diatoms lack the distinct shoulder in the absorption spectrum between 480 and 490 nm due to the high contribution of the light-harvesting pigment, fucoxanthin, which has a much broader absorption peak (Bricaud et al. 2004). Therefore, to minimize the effect of absorption in the MAA bands and infer the contribution of carotenoid pigments to total absorption, we used the spectral absorption ratio of $a_\phi(490)$:$a_\phi(480)$. However, one should be cautious in that this ratio does not distinguish between photoprotective and photosynthetic carotenoids. Figure 12 presents this ratio for the melt water samples and the sea ice vertical profiles. The absorption ratio remained stable and high in the ice melt water. The ratio was also very stable over time in the sea ice; however, a decrease was observed with depth into the sea ice until the bottommost 10 cm where a small increase was observed.

Discussion

Ice-associated environments

Sea ice was permeable during the entire study, i.e., well above a vertical porosity threshold of 5% brine volume content (Golden et al. 2007; Pringle et al. 2009). However, the sea ice tended to retain its salinity well into advanced stages of melt, while low-salinity melt water enveloped the sea ice cover. One explanation for this occurrence is that vertical percolation of melt water through the white ice cover can be restricted by formation of ice as melt water comes in contact with interior temperatures below their freezing point (Eicken et al. 2002; Ehn et al. in press). An additional explanation for the retention of salts in melting sea ice could be related to extracellular polymeric substances (EPS). Exuded in copious amounts by sea ice diatoms (Krembs et al. 2002; Meiners et al. 2003; Riedel et al. 2008) and potentially bacteria (Ewert and Deming 2011), EPS have been shown to retain salt during the freezing of artificial sea ice (Krembs et al. 2001) and act as an anchoring medium for ice diatoms (Krembs and Deming 2008). These findings led Krembs and Deming (2008) to speculate that EPS could play a role in impeding sea ice desalination during melt, as recently documented during ice growth by Krembs et al. (2011).

The impeded exchange of brine in the interior white ice with the ice melt water environment made possible the development of two distinct communities. However, similarities in physical and biological parameters observed between the bottom ice with both the interior ice and ice melt water indicated that some interaction between the ice and ice melt water was occurring. In particular, biological properties specific to the high-light environment associated with melt ponds were observed in the bottom ice. This exchange was largely limited to the bottom 10 cm of the

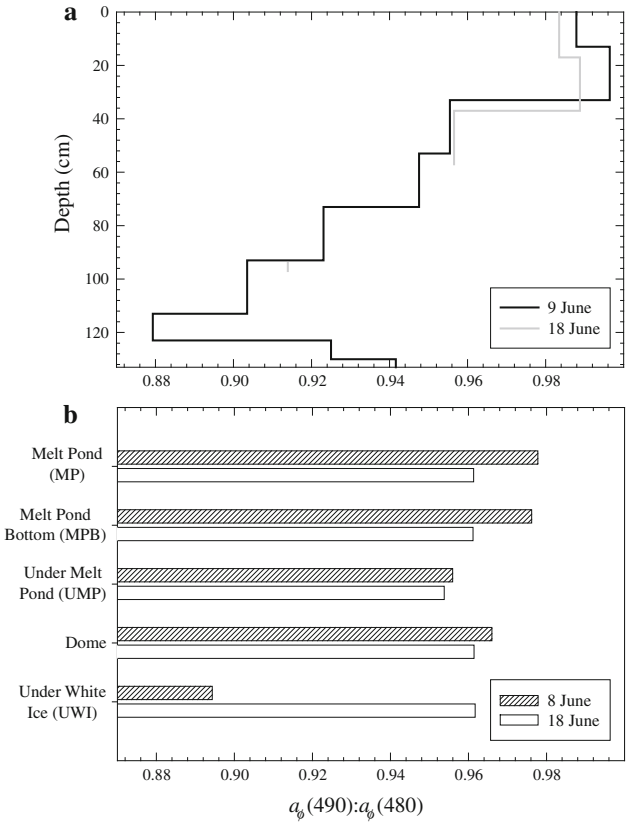

Fig. 12 Values of the spectral absorption ratio, $a_\phi(490):a_\phi(480)$ measured in sea ice (**a**) and ice melt water (**b**) at the beginning and end of the study. The ratio is interpreted as a proxy for the relative contribution to total algal absorption of photoprotective carotenoid pigments, which have a peak and trough absorption at 490 and 480 nm, respectively

sea ice, which agrees with previous observations during advanced stages of melt pond development (Eicken et al. 2002).

Relatively stable sea ice Chl *a* concentrations and correlations of biological properties with brine volume suggested that accumulation of the interior ice algal community was influenced by its confinement to the brine channel network. Interestingly, conservative mixing relationships of the ice melt water samples highlighted that the freshwater ice melt was depleted of nutrients and microbes. Furthermore, these relationships showed that the surface melt ponds were connected to the under-ice melt water, with an important nutrient supply from the seawater. Similar observations have been made in Arctic pack ice (Kramer and Kiko 2010). However, the concentrations of nitrite + nitrate were depleted relative to the seawater. Assuming N-limitation of polar surface seawater in the study region (Tremblay et al. 2008), our results suggest that algal growth in the ice melt water environment was highly N-limited. Due to variability in nitrite + nitrate concentrations in both the bottom ice and the ice melt water, we suggest that sea ice brine could be an important N source to the ice melt water algal community. However, this suggestion will need to be confirmed, as we were unable to distinguish between spatial and temporal variability with the relatively few samples collected.

Community compositions

The interior ice community was distinguished from the ice melt water community by the presence of large-celled algae with a dominance of pennate diatoms. These included common sea ice-associated diatoms (Horner and Schrader 1982; Różańska et al. 2009) that were unique to the sea ice in our study. *Fragilariopsis oceanica* was unique to the ice melt water (dome sample); however, its presence was likely related to its high abundance in an ice-edge phytoplankton bloom that was observed within the underlying water column during the study period (Mundy et al. 2009).

Similarities in the relative composition between the bottom ice and dome samples on June 8–9 (Fig. 10) suggest that the bottom ice algal community could have seeded the ice melt water. Michel et al. (1993) provided evidence that ice algae may seed the sub-ice water column in the Arctic. As EPS have generally been associated with diatoms in the sea ice (Krembs et al. 2002; Meiners et al. 2003; Riedel et al. 2008), it is also plausible that anchoring of the ice-associated diatoms by EPS (Krembs and Deming 2008) may have influenced the unique diatom composition observed within the sea ice. Due to potential brine drainage when sampling the ice core, we further note that this anchoring mechanism could have biased the taxonomic composition of the ice samples toward diatoms. However, due to the relatively high salinities measured in the ice (Ehn et al., in press), we assumed this artifact was minimal. It is further noted that in contrast to the bottom ice community, the relative composition of the dome sample was almost entirely dominated by flagellates on June 18. Therefore, although seeding of the ice melt water from the bottom ice could have played an initial role in determining the ice melt water community composition, a unique community had developed.

High concentrations of picoalgae in the ice melt water on June 8 reflected the highly oligotrophic state of this environment as in warmer waters (Chisholm 1992; Agawin et al. 2000). Covariation of picoalgae with bacteria further suggested a prevalent microbial loop with a dependence of the community on recycled nutrients (Azam et al. 1983). However, Chl *a* concentration and nanoalgae did not demonstrate conservative mixing with the water column. Nanoalgae had increased substantially throughout the ice melt water by the end of the period and were significantly correlated to Chl *a*, suggesting that these algae were

actively accumulating in the melt water and accounted for the majority of algal biomass. Shifts in the relative taxonomic composition of the ice melt water community toward larger flagellates and in numerical dominance from prymnesiophytes to prasinophytes and chrysophytes had also occurred. Interestingly, prymnesiophytes remained the dominant identified photosynthetic flagellates in the sea ice. The dominance of prasinophytes and chrysophytes in the ice melt water agreed closely with the previous studies (Bursa 1963; Gradinger 1996). However, the dominance of the genus *Pyramimonas* was more similar to observations by Gradinger (1996) in Arctic pack ice, where a *Pyramimonas* sp. was found to form a unialgal bloom in an under-ice melt pond. Perhaps, the under-ice pond flora observed by Gradinger (1996) represented a community succession of the ice melt water flora due to an influx of nutrients.

The observations of picocyanobacteria in the interior ice were somewhat surprising. Cyanobacteria are characteristically not abundant in sea ice (Robineau et al. 1994; Meiners et al. 2002) and polar surface waters (Gradinger and Lenz 1989; Robineau et al. 1999; Tremblay et al. 2009), and although a concentration of 900 cells mL^{-1} is small relative to what is encountered in other marine environments, it is relatively high for a polar marine ecosystem. The general paucity of cyanobacteria in the Arctic marine environment has been attributed to low temperatures; however, Robineau et al. (1999) noted many exceptions to this rule, concluding that cyanobacteria can live in cold-temperature marine environments.

The apparent decrease in heterotrophic bacteria by one order of magnitude observed in the sea ice was contrary to the confined nature of the interior ice community and the relatively low abundance of identified bacterial grazers (heterotrophic flagellates and ciliates accounted for <10% of total cell abundance; "Appendix"). Sea ice bacteria have been found to be epiphytic (Smith et al. 1989) and associated with particles in the sea ice (Junge et al. 2004), in particular, attached to EPS (Meiners et al. 2008). Furthermore, observations using DAPI (4′6′-Diamidino-2-phenylindole dihydrochloride) staining confirmed that aggregates of sea ice bacteria were present in a single bottom ice sample collected at the same site as this study (D. Nguyen, pers. obs.). We speculate that the decrease in heterotrophic bacteria was an artifact of the flow cytometry analysis employed in this study. That is, if bacteria were concentrated on larger particles or grouped into larger colonies, they may not have been properly counted because their flow cytometric signature was different from free bacteria. However, if bacteria were more particle associated or colonial in the sea ice, then a potential difference between the interior ice and ice melt water communities is that free-living bacteria play a more important role in the latter.

High-light acclimation

Both the interior ice and the ice melt water communities exist in high-light environments due to their confinement to the ocean surface. Furthermore, the persistent high-pressure atmospheric system observed prior to and during the study resulted in relatively high levels of incident UVR and PAR impinging on the two habitats. Therefore, to survive potentially damaging levels of radiation in these two habitats, we hypothesized that these communities would have photoacclimated.

Important screening compounds include mycosporine-like amino acids (MAAs). The wavelengths of peak UV algal absorption in the data corresponded to the absorption peaks of a variety of MAAs observed in marine algae, such as mycosporine-glycine (310 nm), palythine (320 nm), asternia (330 nm), palythinol (332 nm), porphyra (334 nm), shinorine (334 nm), and palythene (360 nm) (Karentz et al. 1991). However, the very high absorption peaks in the UV range observed in the melt water samples could be an artifact of the method utilized. Freezing filters prior to absorption measurements can cause the release of MAAs from the algal cells into the thawed filters, which decrease the algal cell packaging effect, thereby increasing absorption in the UV range (Sosik 1999; Laurion et al. 2003). Therefore, it is most likely that in situ algal absorption in the UV range was much less than measured on our pre-frozen filters. However, if all MAAs are released into the filter upon freezing and thawing (Laurion et al. 2004), then Chl *a*-specific algal absorption in the UV range can be used to infer a relative contribution of MAAs to total absorption.

The ice melt water community experienced much higher irradiance than the interior white ice community. Within melt ponds, the observed high albedos of both the pond bottom (0.3) and the white ice edge (0.7) (Ehn et al., in press) relative to a typical open water albedo of <0.1 greatly increased radiation levels reaching algae in this habitat. Furthermore, under-ice-transmitted PAR through melt ponds ranged between 38 and 67% of surface radiation in contrast to 5–16% penetrating the white ice cover (Ehn et al. in press). Similarly, the high scattering surface of the white ice would diminish levels of transmitted UVR into the interior ice habitat (Perovich 2006). The much greater peak in UV absorption observed in the averaged ice melt water spectra suggested an enhanced accumulation of MAAs by this community over the interior ice community. This enhancement suggests that the ice melt water community was actively responding to the higher UVR levels.

Specific a^*_ϕ peak wavelengths in the UV range also inferred a different MAA composition produced by the two communities. We surmise that the variability during the

study in algal community composition could have played a role in relative MAA composition, along with possible differences in the irradiance and spectral characteristics of PAR and UVR reaching these communities.

Many carotenoid pigments act as important quenching compounds for highly excited states of Chl *a* and oxygen that occur in microbial cells due to absorption of high UVR and PAR levels (Siefermann-Harms 1987). In our study, a strong contribution of carotenoid pigments to algal absorption was inferred from the carotenoid-related absorption ratio in both the interior ice and the ice melt water communities. Decrease in the ratio with depth into the sea ice suggested a vertical stratification of the interior ice community associated with decreasing light levels as light was attenuated in the ice cover. In addition to sea ice attenuation, community self-shading could have played a role in this vertical stratification (Smith et al. 1988). From the carotenoid absorption ratio increase at the ice bottom, the increased UV peak absorption, and the observed similarities in taxonomic composition between the bottom ice and the ice melt water, we infer a partial infiltration of the ice melt water community into the bottom ice layers.

Conclusions

Freezing and thawing processes associated with sea ice induce a unique level of complexity in polar marine environments resulting in the coexistence of multiple distinct biological communities. In particular, distinctive communities have been described in association with different types of ice melt water, including surface melt pond, under-ice melt pond, and halocline water. During our study, however, these vertically separated habitats did not display unique physical and biological characteristics. We documented only two distinct algal communities: one in the interior ice and one in the ice melt water.

The interior ice community was dominated by diatoms and confined to the limited habitat space of the brine channel network. In contrast, the ice melt water community was suggested to be N-limited and dominated by flagellates. The high-light levels impinging on the ice-associated habitats also induced strong photoprotective responses in both communities as indicated by particulate absorption characteristics. The latter included high absorption in MAA bands and an inferred accumulation of carotenoid pigments, which can play a significant photoprotective role.

Although an ice-edge bloom had produced a high amount of phytoplankton biomass in a very short time in Darnley Bay during the time of our study, it was not significantly incorporated into the pelagic food web (Mundy et al. 2009). Instead, an important contribution of pelagic zooplankton grazers was found near the halocline, where they were likely feeding on the ice-associated algal communities during our study (Hop et al. 2011). Even though the interior ice and ice melt water algal communities had low biomass relative to the ice-edge bloom, they likely represent an ecologically important carbon supply to the ice-covered Arctic food web. A better understanding of the roles the interior ice and ice melt water communities play in the Arctic marine ecosystem is thus warranted, particularly with observations of an earlier and more rapidly melting ice cover (Stroeve et al. 2006; Maslanik et al. 2007) and decreased stratospheric ozone levels in the Arctic (Rex et al. 2004).

Acknowledgments This work is a contribution to the International Polar Year–Circumpolar Flaw Lead system study (IPY–CFL 2008), supported through grants from the Canadian IPY Federal program office, the Natural Sciences and Engineering Research Council and numerous international collaborators. Postdoctoral fellowship support was provided from the Fonds québécois de la recherche sur la nature et les technologies (FQRNT) to C.J.M. and the Centre National d'Études Spatiales (CNES) to J.K.E. Additional funding was provided from the Canadian Museum of Nature to M.P. The participation of H.H. was jointly facilitated by ARCTOS and ArcticNet, within the IPY-project PanAME funded by the Research Council of Norway. We would like to extend our gratitude to Dr. J.-É. Tremblay's lab for processing nutrient samples, A. Rossnagel for CTD data and assistance in the field, and to B. Philippe, M. Palmer, A. Sallon, T. Brown, J. Ferland, S. Pineault, J. Gagnon, J. Martin, D. Nguyen, R. Maranger, and the officers and crew of the CCGS *Amundsen* for logistical and postprocessing support. We gratefully acknowledge K. Meiners and two anonymous reviewers for comments that improved this manuscript.

Appendix

See Table 1.

Table 1 Detailed taxonomic list and abundance (cells mL^{-1}) of unicellular eukaryotes (cells, spores, and cysts) identified and enumerated using inverted microscopy on samples from the interior ice (17–37-cm section from the ice surface collected on June 18), bottom ice (bottommost 3 cm collected on June 9 and 18) and dome (collected on June 8 and 18) collected in Darnley Bay, NT, Canada

Protist group	Interior ice	Bottom ice		Dome	
		June 9 (cells mL^{-1})	June 18 (cells mL^{-1})	June 8 (cells mL^{-1})	June 18 (cells mL^{-1})
Bacillariophyta	**2,018**	**1,096**	**1,070**	**178**	**131**
Coscinodiscophyceae	**741**	**245**	**62**	**45**	**105**
Arcocellulus cornucervis Hasle, von Stosch & Syvertsen	nd	nd	nd	nd	2
Attheya septentrionalis (Østrup) Crawford	nd	16	4	nd	nd
A. cf. *septentrionalis* (Østrup) Crawford	5	nd	nd	nd	nd
Chaetoceros cf. *convolutus* f. *trisetosa* Brunel	nd	nd	4	nd	nd
C. cf. *minimus* (Levander) Marino, Giuffré, Montresor & Zingone	nd	nd	4	1	9
C. neogracile VanLandingham	134	nd	16	nd	9
C. similis Cleve	nd	31	nd	nd	nd
C. simplex Ostenfeld	10	5	nd	nd	nd
C. socialis Lauder (cells)	nd	nd	nd	12	13
C. socialis Lauder (spores)	5	nd	4	4	2
C. tenuissimus Meunier	nd	nd	4	nd	nd
C. vistulae Apstein	134	nd	nd	nd	2
C. wighamii Brightwell	5	nd	nd	nd	nd
Chaetoceros sp. 1	114	131	16	nd	nd
Chaetoceros sp. 2	45	nd	nd	1	46
Chaetoceros spp. (≤5 μm)	159	16	12	2	7
Chaetoceros spp. (6–10 μm)	60	47	nd	3	14
Chaetoceros spp. (≥11 μm)	5	nd	nd	nd	nd
Chaetoceros spp. (hypnospores)	15	nd	nd	nd	nd
Eucampia groenlandica Cleve	nd	nd	nd	4	nd
Thalassiosira nordenskioeldii Cleve	nd	nd	nd	2	nd
Thalassiosira sp. 1	nd	nd	nd	14	nd
Thalassiosira spp. (10–20 μm)	5	nd	nd	1	nd
Thalassiosira spp. (21–50 μm)	45	nd	nd	nd	2
Fragilariophyceae	**nd**	**10**	**27**	**nd**	**nd**
Synedropsis hyperborea (Grunow) Hasle, Medlin & Syvertsen	nd	10	27	nd	nd
Bacillariophyceae	**1,277**	**841**	**981**	**133**	**25**
Cylindrotheca closterium (Ehrenberg) Reimann & Lewin	423	63	27	18	13
Ephemera planamembranacea (Hendey) Paddock	10	nd	16	nd	nd
Fragilariopsis cylindrus (Grunow) Krieger	10	nd	4	nd	nd
F. oceanica (Cleve) Hasle	nd	nd	nd	65	2
Fragilariopsis spp. (10–20 μm)	nd	nd	nd	44	nd
Gyrosigma concilians (Cleve) Okolodkov	nd	31	nd	nd	nd
Navicula gelida Grunow	nd	nd	8	nd	nd
N. gelida var. *radissonii* Poulin & Cardinal	nd	nd	4	nd	nd
N. pagophila var. *manitounukensis* Poulin & Cardinal	nd	26	nd	nd	nd
N. pelagica Cleve	85	nd	333	nd	nd
N. transitans Cleve	10	10	nd	nd	nd
N. transitans var. *derasa* (Grunow) Cleve	nd	16	nd	nd	nd
Navicula spp. (20–50 μm)	10	26	8	nd	nd
Nitzschia frigida Grunow	338	402	120	nd	nd
N. promare Medlin	nd	63	nd	1	nd
Nitzschia spp. (20–50 μm)	10	nd	43	1	nd

Table 1 continued

Protist group	Interior ice	Bottom ice		Dome	
		June 9 (cells mL^{-1})	June 18 (cells mL^{-1})	June 8 (cells mL^{-1})	June 18 (cells mL^{-1})
Nitzschia spp. (>50 μm)	nd	37	8	nd	nd
Pinnularia quadratarea var. *minor* (Østrup) Heiden	nd	16	nd	nd	nd
Pseudogomphonema arcticum (Grunow) Medlin	nd	5	nd	nd	nd
Pseudo-nitzschia cf. *pseudodelicatissima* (Hasle) Hasle	nd	nd	nd	nd	2
Stauroneis radissonii Poulin & Cardinal	nd	nd	16	nd	nd
Pennate sp. 1	40	21	nd	nd	nd
Pennate sp. 2	134	nd	23	nd	nd
Pennate sp. 3	nd	nd	256	nd	nd
Pennate sp. 4	nd	nd	8	nd	nd
Pennate sp. 6	nd	nd	4	nd	nd
Unidentified pennate cells (≤10 μm)	40	21	nd	nd	nd
Unidentified pennate cells (11–20 μm)	129	42	70	2	5
Unidentified pennate cells (21–50 μm)	40	63	31	1	4
Unidentified pennate cells (>50 μm)	nd	nd	4	nd	nd
Dinophyceae	**30**	**16**	**39**	**15**	**29**
Amphidinium spp.	nd	nd	nd	nd	2
Gymnodinium sp. 5	nd	nd	nd	2	nd
Gyrodinium cf. *resplendens* Hulburt	nd	nd	nd	4	nd
Gymnodinium/*Gyrodinium* spp. (10–20 μm)	nd	5	nd	2	18
Gymnodinium/*Gyrodinium* spp. (21–50 μm)	nd	5	nd	6	nd
Heterocapsa arctica Horiguchi	nd	nd	4	nd	nd
H. cf. *niei* (Loeblich III) Morrill & Loeblich III	nd	nd	4	nd	nd
Heterocapsa sp. 2	nd	5	nd	nd	nd
Polarella glacialis Montresor, Procaccini & Stoecker (cyst)	10	nd	27	nd	nd
Protoperidinium bipes (Paulsen) Balech	nd	nd	nd	nd	2
Dinophyceae spp. (10–20 μm)	nd	nd	nd	nd	2
Dinophyceae spp. (21–50 μm)	nd	nd	4	nd	5
Dinophyceae cysts (>50 μm)	20	nd	nd	nd	nd
Chlorophyceae	**10**	**nd**	**nd**	**nd**	**4**
Polytoma spp.	10	nd	nd	nd	nd
Chlorophyceae spp. (11–20 μm)	nd	nd	nd	nd	4
Chrysophyceae	**25**	**37**	**74**	**5**	**449**
Dinobryon balticum (Schütt) Lemmermann	nd	nd	31	nd	216
D. faculiferum (Willén) Willén	nd	nd	8	2	9
Dinobryon spp.	nd	26	8	nd	209
Chrysophyceae spp. (≤5 μm)	nd	10	16	nd	4
Chrysophyceae spp. (6–10 μm)	5	nd	nd	3	9
Chrysophyceae spp. (>10 μm)	5	nd	nd	nd	2
Chrysophyceae cysts	15	nd	12	nd	nd
Dictyochophyceae	**nd**	**10**	**nd**	**5**	**9**
Pseudopedinella spp. (≤5 μm)	nd	10	nd	nd	5
Pseudopedinella spp. (6–10 μm)	nd	nd	nd	5	4
Cryptophyceae	**5**	**10**	**16**	**13**	**32**
Plagioselmis prolonga var. *nordica* Novarino, Lucas & Morrall	nd	nd	nd	nd	2
Cryptophyceae spp. (≤5 μm)	5	10	nd	4	nd
Cryptophyceae spp. (6–10 μm)	nd	nd	16	5	nd

Table 1 continued

Protist group	Interior ice	Bottom ice		Dome	
		June 9 (cells mL^{-1})	June 18 (cells mL^{-1})	June 8 (cells mL^{-1})	June 18 (cells mL^{-1})
Cryptophyceae spp. (>10 μm)	nd	nd	nd	3	30
Euglenophyceae	**nd**	**nd**	**nd**	**3**	**nd**
Euglenophyceae spp. (10–20 μm)	nd	nd	nd	1	nd
Euglenophyceae spp. (>20 μm)	nd	nd	nd	2	nd
Prasinophyceae	**nd**	**52**	**62**	**1**	**229**
Dolichomastix nummulifera Manton	nd	nd	nd	nd	2
Pyramimonas disomata Butcher ex McFadden, Hill & Wetherbee	nd	nd	nd	nd	104
Pyramimonas sp. 1	nd	nd	4	nd	54
Pyramimonas sp. 2	nd	nd	nd	nd	25
Pyramimonas spp. (≤5 μm)	nd	nd	4	1	4
Pyramimonas spp. (6–10 μm)	nd	16	35	nd	30
Pyramimonas spp. (>10 μm)	nd	16	19	nd	11
Prasinophyceae spp. (6–10 μm)	nd	21	nd	nd	nd
Prymnesiophyceae	**40**	**141**	**47**	**64**	**50**
Chrysochromulina spp. (≤5 μm)	15	84	8	16	16
Chrysochromulina spp. (6–10 μm)	20	37	16	42	11
Chrysochromulina spp. (>10 μm)	nd	nd	nd	3	4
Dicrateria/*Imantonia* spp.	nd	nd	nd	2	nd
Prymnesiophyceae sp. 1	nd	nd	nd	nd	2
Prymnesiophyceae spp. (≤5 μm)	5	21	8	1	5
Prymnesiophyceae spp. (6–10 μm)	nd	nd	16	nd	9
Prymnesiophyceae spp. (>10 μm)	nd	nd	nd	nd	4
Unidentified flagellates	**169**	**1,671**	**949**	**203**	**1,212**
Flagellate sp. 2	nd	nd	23	nd	769
Flagellate sp. 3	nd	nd	nd	1	nd
Flagellates (≤5 μm)	119	1,504	748	98	286
Flagellates (6–10 μm)	30	136	101	73	57
Flagellates (11–20 μm)	15	31	70	16	100
Flagellates (>20 μm)	5	nd	8	15	nd
Raphidophyceae	**nd**	**5**	**nd**	**nd**	**2**
Chattonella spp.	nd	nd	nd	nd	2
Raphidophyceae spp. (≥10 μm)	nd	5	nd	nd	nd
Heterotrophic flagellates	**15**	**204**	**43**	**26**	**39**
Bodo cf. *curvifilus* Griessmann	nd	94	nd	nd	nd
Bodo spp.	nd	78	4	1	nd
Leucocryptos marina (Braarud) Butcher	nd	nd	nd	nd	2
Notosolenus sp. sensu Bérard-Therriault et al. (1999)	nd	nd	nd	1	nd
Quadricilia rotundata (Skuja) Vørs	nd	5	nd	nd	nd
Rhynchom nasuta (Stokes) Klebs	5	nd	nd	1	nd
Telonema subtilis Griessmann	10	nd	8	nd	5
Telonema sp. 1	nd	nd	4	11	16
Vanella cf. *simplex* Wolfhart-Bottermann	nd	10	12	nd	nd
Flagellate sp. A	nd	16	nd	nd	14
Heterotrophic flagellates (6–10 μm)	nd	nd	8	nd	2
Heterotrophic flagellates (>10 μm)	nd	nd	8	12	nd
Choanoflagellidea	**nd**	**nd**	**4**	**3**	**46**

Table 1 continued

Protist group	Interior ice	Bottom ice		Dome	
		June 9 (cells mL^{-1})	June 18 (cells mL^{-1})	June 8 (cells mL^{-1})	June 18 (cells mL^{-1})
Bicosta spp.	nd	nd	nd	nd	2
Calliacantha longicaudata (Leadbeater) Leadbeater	nd	nd	nd	nd	2
C. natans (Grøntved) Leadbeater	nd	nd	nd	nd	2
Monosiga sp. sensu Bérard-Therriault et al. (1999)	nd	nd	4	nd	21
Parvicorbicula socialis (Meunier) Deflandre	nd	nd	nd	nd	4
Choanoflagellidea spp. (≤5 μm)	nd	nd	nd	nd	2
Choanoflagellidea spp. (6–10 μm)	nd	nd	nd	1	9
Choanoflagellidea spp. (>10 μm)	nd	nd	nd	2	5
Ciliates	**15**	**5**	**8**	**25**	**7**
Lohmanniella oviformis Leegaard	nd	nd	nd	5	nd
Strombidium spp. (21–50 μm)	5	nd	nd	3	nd
Ciliate sp. 3	nd	nd	nd	5	nd
Ciliates (11–20 μm)	5	5	4	1	2
Ciliates (21–50 μm)	5	nd	4	10	4
Ciliates (>50 μm)	nd	nd	nd	nd	2
Unidentified auto- and heterotrophic cells	**258**	**2,339**	**903**	**54**	**102**
Cyst sp. 1 (17 μm)	nd	nd	4	nd	nd
Cysts (10–20 μm)	5	26	70	1	4
Cysts (21–50 μm)	5	nd	nd	nd	nd
Cell sp. 1 (3–5 μm)	nd	1,535	nd	nd	nd
Unidentified cells (≤5 μm)	189	679	601	26	48
Unidentified cells (6–10 μm)	40	84	147	27	30
Unidentified cells (11–20 μm)	15	10	78	nd	18
Unidentified cells (>20 μm)	5	5	4	nd	2
Presence counts					
Number of species	**20**	**21**	**32**	**18**	**27**
Number of taxa	**52**	**51**	**65**	**54**	**70**

Total abundance of respective taxonomic groups is in bold characters

nd Not detected

References

Agawin NSR, Duarte CM, Agustí S (2000) Nutrient and temperature control of the contribution of picoplankton to phytoplankton biomass and production. Limnol Oceanogr 45:591–600

Apollonio S (1985) Arctic marine phototrophic systems: functions of sea ice stabilization. Arctic 38:167–173

Azam F, Fenchel T, Field JG, Gray JS, Meyer-Reil LA, Thingstad F (1983) The ecological role of water-column microbes in the sea. Mar Ecol Prog Ser 10:257–263

Belzile C, Brugel S, Nozais C, Gratton Y, Demers S (2008) Variations of the abundance and nucleic acid content of heterotrophic bacteria in Beaufort Shelf waters during winter and spring. J Mar Syst 74:946–956. doi:10.1016/j.jmarsys.2007.12.010

Bérard-Therriault L, Poulin M, Bossé L (1999) Guide d'identification du phytoplancton marin de l'estuaire du Saint-Laurent, incluant également certains protozoaires. Publ Spéc Can Sci Halieut Aquat 128:1–387

Bricaud A, Stramski D (1990) Spectral absorption coefficients of living phytoplankton and nonalgal biogenous matter: a comparison between the Peru upwelling area and the Sargasso Sea. Limnol Oceanogr 35:562–582

Bricaud A, Claustre H, Ras J, Oubelkheir K (2004) Natural variability of phytoplanktonic absorption in oceanic waters: influence of the size structure of algal populations. J Geophys Res 109:C11010. doi:10.1029/2004JC002419

Buck KR, Nielsen TG, Hansen BW, Gastrup-Hansen D, Thomsen HA (1998) Infiltration phyto- and protozooplankton assemblages in the annual sea ice of Disko Island, West Greenland, spring 1996. Polar Biol 20:377–381

Bursa A (1963) Phytoplankton in coastal waters of the Arctic Ocean at Point Barrow, Alaska. Arctic 16:239–262

Chisholm SW (1992) Phytoplankton size. In: Falkowski PG, Woodhead AD (eds) Primary productivity and biogeochemical cycles in the sea. Plenum Press, New York, pp 213–237

Cleveland JS, Weidemann AD (1993) Quantifying absorption by aquatic particles: a multiple scattering correction for glass-fiber filters. Limnol Oceanogr 38:1321–1327

Ehn JK, Mundy CJ, Barber DG, Hop H, Rossnagel A, Stewart J (in press) Impact of horizontal spreading on light propagation in

melt pond covered seasonal sea ice in the Canadian Arctic. J Geophys Res. doi:10.1029/2010JC006908
Eicken H, Krouse HR, Kadko D, Perovich DK (2002) Tracer studies of pathways and rates of meltwater transport through Arctic summer sea ice. J Geophys Res 107:C108046. doi:10.1029/2000JC000583
Ewert M, Deming JW (2011) Selective retention in saline ice of extracellular polysaccharides produced by the cold-adapted marine bacterium *Colwellia psychrerythraea* strain 34H. Ann Glaciol 52:111–117
Garrison DL, Buck KR (1986) Organism losses during ice melting: a serious bias in sea ice community studies. Polar Biol 6:237–239
Golden KM, Eicken H, Heaton AL, Miner J, Pringle DJ, Zhu J (2007) Thermal evolution of permeability and microstructure in sea ice. Geophys Res Lett 34:L16501. doi:10.1029/2007GL030447
Gradinger R (1996) Occurrence of an algal bloom under Arctic pack ice. Mar Ecol Prog Ser 131:301–305
Gradinger R (1999) Vertical fine structure of the biomass and composition of algal communities in Arctic pack ice. Mar Biol 133:745–754
Gradinger R, Lenz J (1989) Picocyanobacteria in the high Arctic. Mar Ecol Prog Ser 52:99–101
Gradinger R, Meiners K, Plumley G, Zhang Q, Bluhm BA (2005) Abundance and composition of the sea-ice meiofauna in offshore pack ice of the Beaufort Gyre in summer 2002 and 2003. Polar Biol 28:171–181. doi:10.1007/s00300-004-0674-5
Grasshoff K, Kremling K, Ehrhardt M (1999) Methods of seawater analysis, 3rd edn. Wiley-VCH, New York
Holm-Hansen O, Lorenzen CJ, Holmes RW, Strickland JD (1965) Fluorometric determination of chlorophyll. J Cons Int Explor Mer 30:3–15
Hop H, Mundy CJ, Rossnagel AL, Gosselin M, Barber DG (2011) Zooplankton boom and ice amphipod bust below melting sea ice in the Amundsen Gulf, Arctic Canada. Polar Biol. doi:10.1007/s00300-011-0991-4
Horner RA (2002) A taxonomic guide to some common marine phytoplankton. Biopress Limited, Bristol
Horner R, Schrader GC (1982) Relative contribution of ice-algae, phytoplankton, and benthic microalgae to primary production in nearshore regions of the Beaufort Sea. Arctic 35:485–503
Horner R, Ackley SF, Dieckmann GS, Gulliksen B, Hoshiai T, Legendre L, Melnikov IA, Reeburgh WS, Spindler M, Sullivan C (1992) Ecology of sea ice biota 1. Habitat, terminology, and methodology. Polar Biol 12:417–427
Johnsen G, Samset O, Granskog L, Sakshaug E (1994) In vivo absorption characteristics in 10 classes of bloom-forming phytoplankton: taxonomic characteristics and responses to photoadaptation by means of discriminant and HPLC analysis. Mar Ecol Prog Ser 105:149–157
Junge K, Eicken H, Deming JW (2004) Bacterial activity at −2 to −20°C in Arctic wintertime sea ice. Appl Environ Microbiol 70:550–557. doi:10.1128/AEM.70.1.550-557.2004
Karentz D, McEuen FS, Land MC, Dunlap WC (1991) Survey of mycosporine-like amino acid compounds in Antarctic marine organisms: potential protection from ultraviolet exposure. Mar Biol 108:157–166
Kashino Y, Fujimoto K, Akamatsu A, Koike H, Satoh K, Kudoh S (1998) Photosynthetic pigment composition of ice algal and phytoplankton assemblages in early spring in Saroma Ko Lagoon, Hokkaido, Japan. Proc NIPR Symp Polar Biol 11:22–32
Kirk JTO (1994) Light and photosynthesis in aquatic ecosystems, 2nd edn. Cambridge University Press, Cambridge
Kramer M, Kiko R (2010) Brackish meltponds on Arctic sea ice—a new habitat for marine metazoans. Polar Biol. doi:10.1007/s00300-010-0911-z
Krembs C, Deming JW (2008) The role of exopolymers in microbial adaptation to sea ice. In: Margesin R, Schinner F, Marx JC, Gerday C (eds) Psychrophiles: from biodiversity to biotechnology. Springer, New York, pp 247–264
Krembs C, Mock T, Gradinger R (2001) A mesocosm study on physical-biological interactions in artificial Arctic sea ice. Polar Biol 24:356–364
Krembs C, Eicken H, Junge K, Deming JW (2002) High concentrations of exopolymeric substances in Arctic winter sea ice: implications for the polar ocean carbon cycle and cryoprotection of diatoms. Deep Sea Res I 49:2163–2181. doi:10.1016/S0967-0637(02)00122-X
Krembs C, Eicken H, Deming JW (2011) Exopolymer alteration of physical properties of sea ice and implications for ice habitability and biogeochemistry in a warmer Arctic. Proc Natl Acad Sci USA. doi:10.1073/pnas.1100701108
Kudoh S, Imura S, Kashino Y (2003) Xanthophyll-cycle of ice algae on the sea ice bottom in Saroma Ko lagoon, Hokkaido, Japan. Polar Biosci 16:86–97
Laurion I, Blouin F, Roy S (2003) The quantitative filter technique for measuring phytoplankton absorption: interference by MAAs in the UV waveband. Limnol Oceanogr Methods 1:1–9
Laurion I, Blouin F, Roy S (2004) Packaging of mycosporine-like amino acids in dinoflagellates. Mar Ecol Prog Ser 279:297–303
Leu E, Wiktor J, Søreide JE, Berge J, Falk-Petersen S (2010) Increased irradiance reduces food quality of sea ice algae. Mar Ecol Prog Ser 411:49–60. doi:10.3354/meps08647
Lund JWG, Kipling C, Le Cren ED (1958) The inverted microscope method of estimating algal number and the statistical basis of estimations by counting. Hydrobiologia 11:143–170
Manes SS, Gradinger R (2009) Small scale vertical gradients of Arctic ice algal photophysiological properties. Photosynth Res 102:53–66. doi:10.1007/s11120-009-9489-0
Marie D, Simon N, Vaulot D (2005) Phytoplankton cell counting by flow cytometry. In: Andersen RA (ed) Algal culturing techniques. Academic Press, London, pp 253–268
Maslanik JA, Fowler C, Stroeve J, Drobot S, Zwally J, Yi D, Emery W (2007) A younger, thinner Arctic ice cover: increased potential for rapid extensive sea-ice loss. Geophys Res Lett 34:L24501. doi:10.1029/2007GL0320432007
Medlin LK, Hasle GR (1990) Some *Nitzschia* and related diatom species from fast ice samples in the Arctic and Antarctic. Polar Biol 10:451–479
Meiners K, Fehling J, Granskog MA, Spindler M (2002) Abundance, biomass and composition of biota in Baltic sea ice and underlying water (March 2000). Polar Biol 25:761–770. doi:10.1007/s00300-002-0403-x
Meiners K, Gradinger R, Fehling J, Civitarese G, Spindler M (2003) Vertical distribution of exopolymer particles in sea ice of the Fram Strait (Arctic) during autumn. Mar Ecol Progr Ser 248:1–13
Meiners K, Krembs C, Gradinger R (2008) Exopolymer particles: microbial hotspots of enhanced bacterial activity in Arctic fast ice (Chukchi Sea). Aquat Microb Ecol 52:195–207. doi:10.3354/ame01214
Melnikov IA, Kolosova EG, Welch HE, Zhitina LS (2002) Sea ice biological communities and nutrient dynamics in the Canada Basin of the Arctic Ocean. Deep Sea Res I 49:1623–1649
Michel C, Legendre L, Therriault J-C, Demers S, Vandevelde T (1993) Springtime coupling between ice algal and phytoplankton assemblages in Southeastern Hudson Bay, Canadian Arctic. Polar Biol 13:441–449
Mundy CJ, Gosselin M, Ehn JK, Gratton Y, Rossnagel AL, Barber DG, Martin J, Tremblay J-É, Palmer M, Arrigo K, Darnis G, Fortier L, Else B, Papakyriakou TN (2009) Contribution of under-ice primary production to an ice-edge upwelling

phytoplankton bloom in the Canadian Beaufort Sea. Geophys Res Lett 36:L17601. doi:10.1029/2009GL038837
Parsons TR, Maita Y, Lali CM (1984) A manual of chemical and biological methods for seawater analysis. Pergamon Press, Toronto
Perovich DK (2005) On the aggregate-scale partitioning of solar radiation in Arctic sea ice during the Surface Heat Budget of the Artic Ocean (SHEBA) field experiment. J Geophy Res 110:C03002. doi:10.1029/2004JC002512
Perovich DK (2006) The interaction of ultraviolet light with Arctic sea ice during SHEBA. Ann Glaciol 44:47–52
Petrich C, Eicken H (2010) Chapter 2. Growth, structure and properties of sea ice. In: Thomas DN, Dieckmann GS (eds) Sea ice, 2nd edn. Wiley Blackwell Publishing, Oxford. doi:10.1002/9781444317145.ch2
Poulin M (1990) Ice diatoms: the Arctic. In: Medlin LK, Priddle J (eds) Polar marine diatoms. British Antarctic Survey, Cambridge, pp 15–18
Poulin M (1991) Sea ice diatoms (Bacillariophyceae) of the Canadian Arctic. 2. A taxonomic, morphological and geographical study of *Gyrosigma concilians*. Nord J Bot 10:681–688
Poulin M, Cardinal A (1982) Sea ice diatoms from Manitounuk Sound, southeastern Hudson Bay (Quebec, Canada). II. Naviculaceae, genus *Navicula*. Can J Bot 60:2825–2845
Pringle DJ, Miner JE, Eicken H, Golden KM (2009) Pore space percolation in sea ice single crystals. J Geophys Res 114: C12017. doi:10.1029/2008JC005145
Rex M, Salawitch RJ, von der Gathen P, Harris NRP, Chipperfield MP, Naujokat B (2004) Arctic ozone loss and climate change. Geophys Res Lett 31:L04116. doi:10.1029/2003GL018844
Riedel A, Michel C, Gosselin M, LeBlanc B (2008) Winter–spring dynamics in sea-ice carbon cycling in the coastal Arctic Ocean. J Mar Syst 74:918–932. doi:10.1016/j.jmarsys.2008.01.003
Robineau B, Legendre L, Therriault J-C, Fortier L, Rosenberg G, Demers S (1994) Ultra-algae (5 μm) in the ice, at the ice-water interface and in the under-ice water column (southeastern Hudson Bay, Canada). Mar Ecol Prog Ser 115:169–180
Robineau B, Legendre L, Michel C, Budeus G, Kattner G, Schneider W, Pesant S (1999) Ultraphytoplankton abundances and chlorophyll *a* concentrations in ice-covered waters of northern seas. J Plankton Res 21:735–755
Roy S (2000) Strategies for the minimisation of UV-induced damage. In: de Mora SJ, Demers S, Vernet M (eds) The effects of UV radiation in the marine environment. Cambridge University Press, Cambridge, pp 177–205
Różańska M, Gosselin M, Poulin M, Wiktor JM, Michel C (2009) Influence of environmental factors on the development of bottom ice protist communities during the winter–spring transition. Mar Ecol Prog Ser 386:43–59. doi:10.3354/meps08092
Siefermann-Harms D (1987) The light-harvesting and protective functions of carotenoids in photosynthetic membranes. Physiol Plantarium 69:561–568
Smith REH, Anning J, Clement P, Cota G (1988) Abundance and production of ice algae in Resolute Passage, Canadian Arctic. Mar Ecol Prog Ser 48:251–263
Smith REH, Clement P, Cota G (1989) Population dynamics of bacteria in Arctic sea ice. Microb Ecol 17:63–76
Smith REH, Harrison WG, Harris LR, Herman AW (1990) Vertical fine structure of particulate matter and nutrients in sea ice of the high Arctic. Can J Fish Aquat Sci 47:1348–1355
Sosik HM (1999) Storage of marine particulate samples for light-absorption measurements. Limnol Oceanogr 44:1139–1141
Stroeve J, Markus T, Meier WN, Miller J (2006) Recent changes in the Arctic melt season. Ann Glaciol 44:367–374. doi:10.3189/172756406781811583
Stuart V, Sathyendranath S, Head EJH, Platt T, Irwin B, Maass H (2000) Bio-optical characteristics of diatom and prymnesiophyte populations in the Labrador Sea. Mar Ecol 201:91–106
Syvertsen EE (1991) Ice algae in the Barents Sea: types of assemblages, origin, fate and role in the ice-edge phytoplankton bloom. Polar Res 10:277–287
Throndsen J, Hasle GR, Tangen K (2007) Phytoplankton of Norwegian coastal waters. Almater Forlag AS, Oslo
Tomas CR (1997) Identifying marine phytoplankton. Academic Press, San Diego
Tremblay J-É, Simpson K, Martin J, Miller L, Gratton Y, Barber D, Price NM (2008) Vertical stability and the annual dynamics of nutrients and chlorophyll fluorescence in the coastal, southeast Beaufort Sea. J Geophys Res 113:C07S90. doi:10.1029/2007JC004547
Tremblay G, Belzile C, Gosselin M, Poulin M, Roy S, Tremblay J-É (2009) Late summer phytoplankton distribution along a 3,500 km transect in Canadian Arctic waters: strong numerical dominance by picoeukaryotes. Aquat Microb Ecol 54:55–70
Uusikivi J, Vähätalo AV, Granskog MA, Sommaruga R (2010) Contribution of mycosporine-like amino acids and colored dissolved and particulate matter to sea ice optical properties and ultraviolet attenuation. Limnol Oceanogr 55:703–713
von Quillfeldt CH (2000) Common diatom species in Arctic spring blooms: their distribution and abundance. Bot Mar 43:499–516
von Quillfeldt CH (2001) Identification of some easily confused common diatom species in Arctic spring blooms. Bot Mar 44:375–389